Journal of the European Ceramic Society xxx (xxxx) xxx–xxx

Contents lists available at ScienceDirect

Journal of the European Ceramic Society

journal homepage: www.elsevier.com/locate/jeurceramsoc

Original Article

A thermodynamic approach to surface modification of calcium phosphate implants by phosphate evaporation and condensation

Nicola Döbelin[a,*], Yassine Maazouz[a], Roman Heuberger[a], Marc Bohner[a], Ashley A. Armstrong[b], Amy J. Wagoner Johnson[c], Christoph Wanner[d]

[a] RMS Foundation, Bischmattstrasse 12, 2544, Bettlach, Switzerland
[b] Department of Mechanical Science and Engineering, Grainger College of Engineering, University of Illinois at Urbana-Champaign, Urbana, IL, 61801, USA
[c] Department of Mechanical Science and Engineering, Grainger College of Engineering, Carle Illinois College of Medicine, and Carl R. Woese Institute for Genomic Biology, University of Illinois at Urbana-Champaign, Urbana, IL, 61801, USA
[d] Institute of Geological Sciences, University of Bern, Baltzerstrasse 1-3, 3012, Bern, Switzerland

ARTICLE INFO

Keywords:
Calcium phosphate
Evaporation
Surface modification
Bioceramics

ABSTRACT

It has been reported in the literature that thermal treatment of calcium phosphate ceramics chemically alters the surface composition by phosphate evaporation. To predict the compositional changes, we have developed a thermodynamic model for the evaporation of phosphorous species from CPP, TCP, HA, and TetCP. In an open atmosphere, the model predicts the formation of a surface layer consisting of a sequence of increasingly phosphate-depleted phases. In a closed system, the atmosphere reaches equilibrium with a single-phase surface layer. To verify our model, we performed a series of experiments which confirmed the predicted formation of phosphate-depleted surface layers. These experiments further demonstrated that controlled supersaturation of the atmosphere led to formation of a phosphate-enriched surface layer as a result of phosphate condensation. In conclusion, our thermodynamic model is capable of predicting the surface modification by phosphate evaporation and condensation of calcium phosphate phases during high-temperature processing in different environments.

1. Introduction

The surface chemistry of biomaterials has long been regarded as being of utmost importance for the interaction of the host organism with the implant [1,2]. It is assumed that the surface composition is decisive for the behaviour of implanted materials due to the chemical interactions occurring at the interface with biological tissues and fluids, including dissolution and ion release, as well as precipitation of a biomimetic apatite layer. Surface chemistry is thus important to all biomaterials and has been studied extensively for metals [3], polymers [4], and ceramics [5]. However, calcium phosphate research has mostly focused on bulk-compositional, morphological, and topographical aspects and their influence on the bone regeneration capacity [6]. The surface chemistry of low-temperature phases, such as nonstoichiometric apatites has been explored in depth [7,8], but that of high-temperature CaP phases has been scarcely studied. The effect of surface chemistry on the immune response and bone healing process is also poorly understood.

The majority of calcium phosphate (CaP) products used clinically as bone graft substitutes are based on the relatively insoluble phases hydroxyapatite (HA, $Ca_5(PO_4)_3OH$), β-tricalcium phosphate (β-TCP, $Ca_3(PO_4)_2$), or biphasic mixtures thereof (BCP) [9]. The products are most commonly applied in the form of highly porous granules or scaffolds [10]. HA and β-TCP show good osteointegration, and while HA is not resorbable, β-TCP is generally actively resorbed by osteoclasts [11,12]. Both phases can be obtained by decomposition or solid-state reactions of a variety of precursor phases at a high temperature. A sintering step at 1000 °C or above is often also employed to consolidate the product and improve its mechanical properties [13]. It can therefore be assumed that most commercially available HA, β-TCP, and BCP bone void filling products have at some point along their production process been subjected to a thermal treatment above 1000 °C. The Ca and P content is considered to be unaffected by these temperatures. Only the structural components H^+, OH^-, H_2O, CO_3^{2-}, and organic residues are removed, typically resulting in the release of gaseous H_2O or CO_2. Thermal treatment at 1000 °C is even recommended in ISO 13779 [14] for quantitative determination of the Ca:P ratio. It was, however, mentioned early on by Welch and Gutt [15] that phosphate

* Corresponding author.
E-mail address: nicola.doebelin@rms-foundation.ch (N. Döbelin).

https://doi.org/10.1016/j.jeurceramsoc.2020.07.028
Received 10 February 2020; Received in revised form 6 July 2020; Accepted 13 July 2020

species evaporate from Ca-pyrophosphate (CPP, $Ca_2P_2O_7$) and TCP at high temperatures. The same observation was later confirmed for CPP, TCP, and also for tetracalcium phosphate (TetCP, $Ca_4(PO_4)_2O$) by Nagai et al. [16,17], who reported that the dominant volatile species released from the surface were PO, P_2, and PO_2. The absolute amount of phosphate removed by evaporation may be negligible in relation to the bulk composition and possibly remain below the detection limits of most analytical techniques, which would explain why it is commonly ignored. But considering that the phosphate depletion is concentrated at the surface, it likely has a substantial effect on the local environment at the implantation site. Variations in surface chemistry resulting from variable thermal processing conditions of otherwise identical samples might thus explain inconsistencies in biological behaviour reported in the literature. For instance, β-TCP has been reported to be both bioactive [18] and non-bioactive [19], non-osteoinductive [20] and highly osteoinductive [21,22], highly resorbable [20,23] and poorly resorbable [23]. Authors have related this dichotomous behaviour with the effect of sintering temperature on specific surface area, bulk composition, and scaffold or pore topography. The effects of calcination on the solubility and reactivity of CaP materials have been systematically investigated [24], and the influence of the resulting surface modification on cell activity has been experimentally confirmed [25]. However, to the best of our knowledge, no attempt has yet been made to describe the chemical changes systematically and in accordance with the thermodynamic properties of the CaP phases. The present work is the first attempt to study the extent and impact of phosphate evaporation on the surface composition of CaP phases upon different types of thermal treatment, broadening our understanding of the biointerface in the field of bone graft substitutes. For this purpose, we have developed a thermodynamic model for the decomposition of CPP, TCP, HA, and TetCP by phosphate evaporation that allows us to precisely understand and predict the surface composition of thermally treated CaP implants. The calculations were made for the temperature range of 298–1700 K and for open and closed atmospheres at a H_2O vapour pressure of 1.50 kPa, and the validity of the model was verified by a series of experiments.

2. Materials and methods

2.1. Thermodynamic model

A list of all possible decomposition reactions of the solid phases CPP, TCP, HA, and TetCP by release of one of the volatile P species P, P_2, P_4, PO, PO_2, P_4O_6, or P_4O_{10} was compiled (Table S1). Solid decomposition products were TCP, HA, TetCP, or CaO. In order to determine whether a specific reaction is thermodynamically favourable, Gibbs free energies of reaction ΔG_r were calculated for the temperature range between 298 and 1700 K. To do so, temperature dependent Gibbs free energies of formation ΔG_f° of all solid and gas phases were taken from the literature (Table S2). Subsequently, for reactions where a solid A decomposes to a solid B and two gas species C and D (Eq. (1), with α-δ denoting stoichiometric coefficients), the Gibbs free energy of reaction at the standard state ΔG_r° was calculated according to Eq. (2).

$$\alpha A(s) \rightarrow \beta B(s) + \gamma C(g) + \delta D(g) \tag{1}$$

$$\Delta G_r^0 = \beta \cdot \Delta G_{f,B}^0 + \gamma \cdot \Delta G_{f,C}^0 + \delta \cdot \Delta G_{f,D}^0 - \alpha \cdot \Delta G_{f,A}^0 \tag{2}$$

Finally, the Gibbs free energy of reaction ΔG_r was calculated for the more general case where the fugacity of gas species f (i.e. the thermodynamically effective gas pressure given in bar) deviates from its 1 bar standard state f^0 according to Eq. (3).

$$\Delta G_r = \Delta G_r^0 + R \cdot T \cdot \ln(Q) \tag{3}$$

R and T are the ideal gas constant and temperature, respectively, and Q refers to the reaction quotient. For Eq. (1), Q is defined as

$$Q = \frac{(a_B)^\beta \cdot (a_C)^\gamma \cdot (a_D)^\delta}{(a_A)^\alpha} \tag{4}$$

where a_A and a_B denote the activity of solids A and B, and a_C and a_D refer to the activity of gases C and D. While the activity of pure solids is 1.0 by definition, the activity of a gas species is defined as the ratio between the fugacity f at the pressure of interest and the 1 bar standard state f° ($a_{gas} = f/f^\circ = f$). Thus, in Eq. (4) both solid and gas species activities are dimensionless numbers and the activity of gas species is equal to the value of f. Since the pressure of interest in our system is 1 bar only, it is safe to assume ideal behaviour for all gas species involved, which means that their fugacities are nearly identical to the corresponding partial pressures. Thus, to calculate the reaction quotient Q, the fugacity of O_2 was set to the atmospheric pressure of 0.2095 bar, and the fugacity of the volatile phosphate species was set to 10^{-300} bar, assuming that the partial pressure of the phosphate species at the beginning of the decomposition reaction is nearly 0 kPa. This value was the smallest value processed as non-zero by Microsoft Excel (version 2016), thus avoiding computational errors caused by *ln(0)*. For reactions releasing H_2O, the fugacity of H_2O(g) was set to 0.015 bar, which corresponded to a relative humidity of 50 % at 298 K.

For the decomposition reactions listed in Table S1, reaction components C and D in Eqs. (1)–(5) typically represent volatile P species (C) and O_2 (D), respectively. At chemical equilibrium, ΔG_r as defined in Eq. (3) is equal to zero and Q is equivalent to the equilibrium constant K_f. Consequently, the equilibrium (i.e. saturation) vapour pressures P_C (bar) of the P gas species was calculated for all reactions by rearranging Eq. (4) to Eq. (5).

$$a_C = f_C = P_C = \left(\frac{K_f}{a_D^\delta}\right)^{\frac{1}{\gamma}} \tag{5}$$

To do so, all activities of solid phases were again taken as 1.0, while the fugacities of O_2(g) and H_2O(g) (if involved) were again set to 0.2095 and 0.015 bar, respectively. K_f was determined by setting ΔG_r to zero and rearranging Eq. (3) to

$$K_f = \exp\left(-\frac{\Delta G_r^0}{R \cdot T}\right) \tag{6}$$

To assess whether the solid-state reactions occur among the substrate and the solid reaction product resulting from the evaporation of P gas species (Table S1), reaction energies ΔG_r of possible solid-state reactions (Table S3) were calculated following the principles of Eqs. (1)–(3), again assuming activities of solid phases to be 1.0 and the fugacity of H_2O(g) (if involved) to be constant at 0.015 bar. The reactions were normalized to 1 mol of the Ca-rich phase, assuming that its availability was limited by the decomposition rate, whereas the availability of the phosphate-rich substrate was unlimited.

A model for thermal decomposition by phosphate evaporation was derived from the results of the thermodynamic calculations under the following presumptions:

1 Evaporation occurs for decomposition reactions with negative reaction energies ($\Delta G_r < 0$).
2 In case of $\Delta G_r > 0$, the direction of the decomposition reaction reverts to a condensation reaction.
3 Solid-state reactions occur if the reaction energy is negative and if the solid phases are in direct contact.
4 In an open system, the atmosphere is constantly flushed and partial pressures of all P gas species remain below saturation.
5 In a closed system, partial pressures of all P gas species can reach saturation.

Our model does not consider kinetic parameters such as activation energies, reaction rates, nucleation rates, or specific surface areas.

Table 1
Reference materials used for verification experiments. CDHA refers to Ca-deficient hydroxyapatite ($Ca_{10-x}(HPO_4)_x(PO_4)_{6-x}(OH)_{2-x}$) with a variable Ca content.

Material designation	Raw materials	Supplier	Pre-processing
CaP1.0r	DCPA	Merck, Darmstadt, Germany	–
CaP1.0p	DCPA	Merck, Darmstadt, Germany	24 h at 673 K
CaP1.5	CDHA	Plasma Biotal, Tideswell Buxton, UK	–
CaP1.6	CDHA	Brenntag Schweizerhalle, Basel, Switzerland	–
CaP1.65	$CaCO_3$	VWR International GmbH, Dietikon, Switzerland	1h at 1173K
	DCPA	Jost Chemical Co., St. Louis, USA	
CaP1.7	$CaCO_3$	VWR International GmbH, Dietikon, Switzerland	1h at 1173K
	DCPA	Jost Chemical Co., St. Louis, USA	
CaO	Ca-hydroxide	KFN, Netstal, Switzerland	–

2.2. Experimental verification

The thermodynamic model was validated experimentally by exposing reference samples of five different Ca:P ratios to high temperatures in two different atmospheres. Afterwards the phase composition at the sample surface was quantified and compared to the bulk composition to determine changes of the Ca:P ratio resulting from phosphate evaporation or condensation. As shown in Table 1, the reference materials CaP1.0, CaP1.5, CaP1.6, CaP1.65 and CaP1.7, designated according to their approximate initial molar Ca:P ratio, comprised precipitated materials which had never been subjected to thermal treatments prior to the evaporation experiments, as well as pre-processed materials. Specifically, material CaP1.0 was tested in raw condition (CaP1.0r) and after pre-processing at 673 K for 24 h (CaP1.0p) to assess the effect of relatively large quantities of H_2O released from the raw material (DCPA, $CaHPO_4$) to the furnace atmosphere upon dehydration.

In the first series of experiments, disks of 30 mm in diameter and 2–4 mm thickness were prepared from the CaP materials listed in Table 1 using a manual uniaxial press (Perkin-Elmer, Überlingen, Germany). The pressure was adjusted to the different materials in the range from 42 to 141 MPa to obtain mechanically stable disks but avoid cracking or chipping during extrusion from the pressure mould. Single material samples were then placed in a furnace (Nabertherm, Härkingen, Switzerland) in stacks of three and heated to 1373 K for 36 h. Up to 10 stacks were spread on the basal plate of the furnace as shown in Fig. 1. The furnace was constantly flushed with a stream of fresh air to avoid saturation of volatile P species in the atmosphere. Afterwards, the phase composition of the top and bottom surface of the top disks were determined by X-ray powder diffraction (XRD) in reflective geometry directly on the disks' surfaces using a D8 Advance diffractometer (Bruker, Karlsruhe, Germany) with Cu$K\alpha$ radiation. The footprint of the X-ray beam on the sample surface was 15 × 15 mm, and a range from 4 to 60° 2θ was scanned with a step size of 0.0122°. Phase quantities were determined by Rietveld refinement with the software Profex [26]. A depth profile of the molar Ca:P ratio was determined by XPS on a cross section through the disks. The measurements were performed with a Kratos Axis Nova (Kratos Analytical, Manchester, UK) using monochromatic Al$K\alpha$-irradiation (1486.7 eV), 225 W and angle of incidence 54.6°. Areas of a nominal diameter of 110 µm were analysed

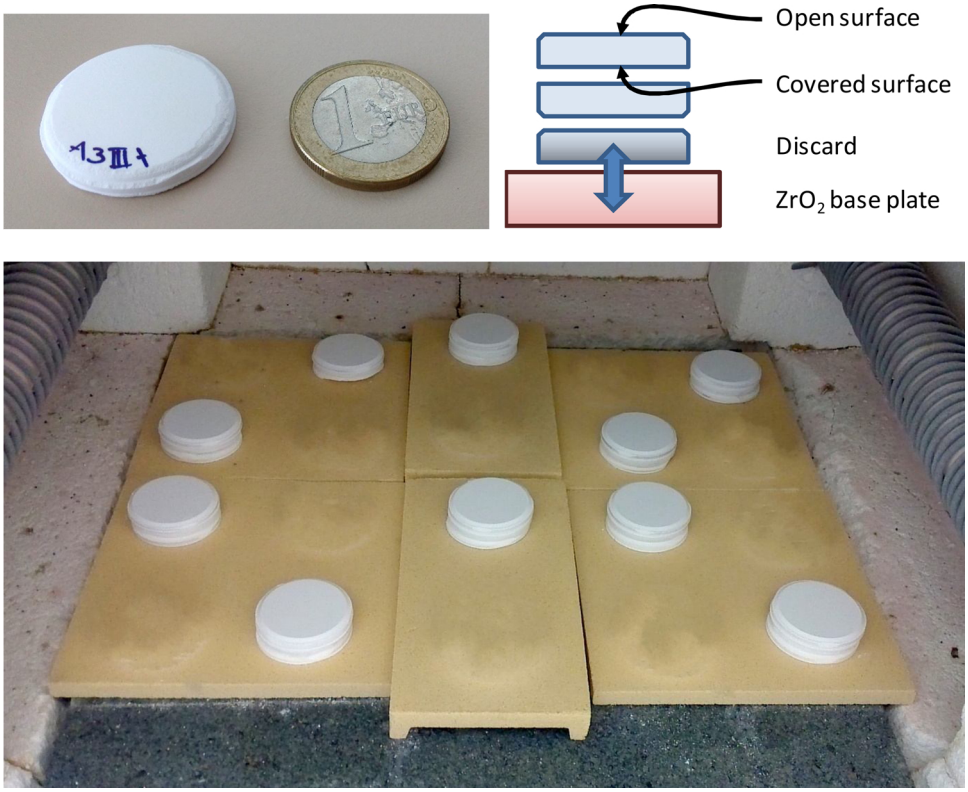

Fig. 1. Disks the size of a coin were placed in the furnace in stacks of three. Only the surface composition of the top disks was analysed. The bottom and middle disks were used to protect the top disk from interaction with the base plate and were discarded after the thermal treatment.

Fig. 2. Stacked disks surrounded by loose CaP1.0r powder for the second round of experiments in the closed furnace.

perpendicular to the sample surface. The areas were positioned on a line in order to measure a concentration profile over the cross section. The spectra were analysed using CasaXPS Software (Version 2.3.20, Casa Software Ltd., Devon, UK). Peak shifting was corrected by referencing aliphatic carbon to 285 eV. The areas of the peaks were determined after subtraction of an iterated Shirley background and correction by the sensitivity factors given by Kratos. The Ca:P ratio was calculated assuming a homogenous compound.

In the second round of experiments, disks of materials CaP1.5, CaP1.6, CaP1.65, CaP1.7, and CaO (Table 1) were placed in the furnace in a similar arrangement as described above. In addition, lose powder of material CaP1.0r was placed in the furnace in circles around the stacked disks, carefully avoiding physical contact with the disks (Fig. 2). The purpose of this setup was to study the evaporation of P species from the CaP1.0 powder and condensation on the surface of the disks. The samples were processed at 1373 K for 36 h in a static atmosphere to allow saturation of the evaporated gas species. The phase composition of the top and bottom surface of the top disks were analysed by XRD as described above.

The third round of experiments aimed at analysing the effect of calcination temperature on the evaporation. Stacked disks of material CaP1.0r were placed in the flushed furnace and processed for 36 h at either 1073 K, 1273 K, or 1373 K. The composition of the top surface was analysed by XRD as described above. Finally, the fourth experimental series analysed the effect of calcination time in a similar arrangement. Stacked disks of material CaP1.0r were calcined at 1373 K for 2.25, 4.5, 9, 18, 36, and 72 h in the flushed furnace, followed by XRD analysis of the top surface.

Differences between the surface and bulk compositions of the processed samples were tested for significance using a heteroscedastic *t*-test in Microsoft Excel (version 2016). Significant factors were determined in a two-way ANOVA using Minitab (version 19). Factors included A: sample surface (top / bottom), and B: furnace position (rear-left / center-center / front-right) to test for a significant response of the Ca:P ratio at the top surface relative to the bottom surface. The ANOVA was performed separately in open furnace atmosphere for materials CaP1.0r, CaP1.0p, CaP1.5, CaP1.6, CaP1.65, and CaP1.7, and in closed furnace atmosphere for CaP1.5, CaP1.6, CaP1.65, CaP1.7, and CaO. In addition, the significance of pre-treatment of material CaP1.0 was determined using factors A: pre-treatment (no / yes) and B: furnace position, by testing for a significant response of the Ca:P ratio at the top surface of CaP1.0p relative to CaP1.0r.

3. Results

3.1. Thermodynamic calculations

Gibbs free energies of reaction ΔG_r of all possible decomposition reactions of CPP at an initial partial pressure of the P gasses of 10^{-298} kPa are shown in Fig. 3. Results for the decomposition reactions of TCP, HA, and TetCP are shown in the supplementary Figs. S1–S9. The majority of decomposition reactions are thermodynamically favourable ($\Delta G_r < 0$) at and above 298 K. However, some gas species are supersaturated ($\Delta G_r > 0$) below 800 K at a partial pressure of 10^{-298} kPa. Lower partial pressures could not be used for direct calculation of ΔG_r due to software limitations (values smaller than 10^{-300} bar were treated as 0 by Microsoft Excel version 2016, causing a *ln(0)* error in the calculation of ΔG_r), but extrapolation of ΔG_r in the logarithmic pressure domain showed that below a partial pressure of 10^{-1740} kPa all decomposition reactions considered in this study (Table S1) were thermodynamically favourable at and above room temperature.

The calculated equilibrium vapour pressures of all CPP decomposition reactions are presented in Fig. 4. Values for decomposition of TCP, HA, and TetCP are given in supplementary Figs. S10–S18. All gas species showed a very strong temperature dependency and PO_2 reached the highest partial pressure in all phase systems. The calculated saturation pressures were generally very low. The highest value determined was for the reaction CPP → TCP + PO_2 at 1700 K and it was $4.98 \cdot 10^{-4}$ kPa. All other values were orders of magnitude lower, indicating that in a closed system only a small absolute amount of phosphate evaporates before saturation is reached.

The observation that for all solid phases the calculated ΔG_r were most negative when PO_2(g) was formed as P-gas species (Figs. 3, S1–S9) thus demonstrated that at the given O_2 fugacity, all P gases react with O_2(g) until PO_2(g) is formed as the final gaseous reaction product. This is further manifested by the highest saturation vapour pressures obtained for PO_2(g) and that these are at least five orders of magnitude higher than those of other P-gas species (Figs. 4, S10–S18). Consequently, our calculations demonstrate that a mixture of different P gas species is thermodynamically not stable at an atmospheric O_2 partial pressure of 20.95 kPa.

Calculated reaction energies ΔG_r for solid-state reactions with CPP

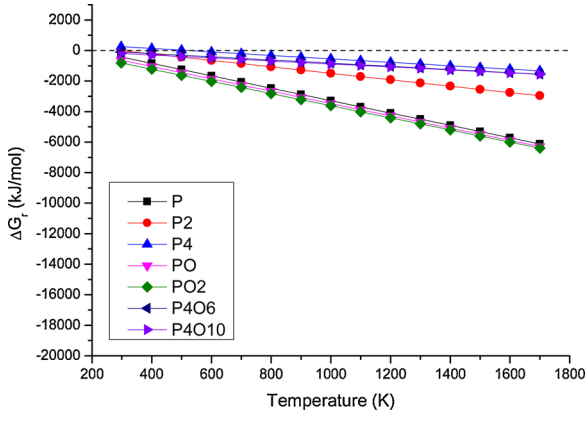

Fig. 3. Calculated Gibbs free energies of reaction for the decomposition of CPP → TCP + gas at a partial pressure of the gas species of 10^{-298} kPa.

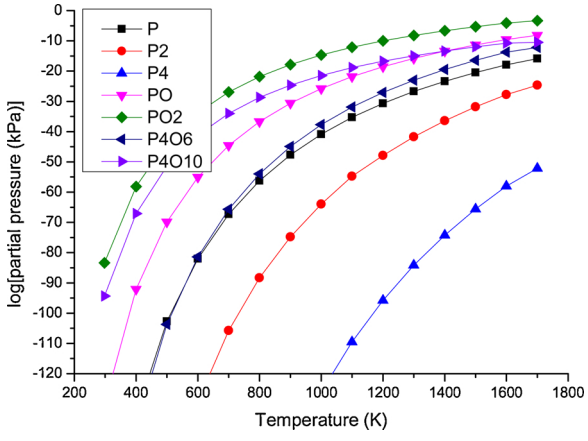

Fig. 4. Calculated saturation partial pressures for P gas species in equilibrium with CPP + TCP.

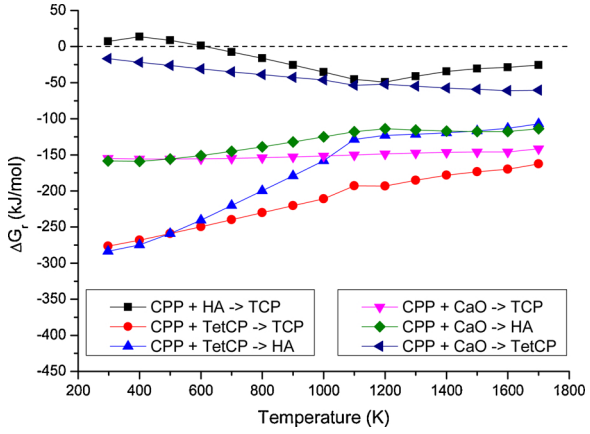

Fig. 5. Calculated Gibbs free energies of reaction ΔG_r of CPP solid-state reactions.

are shown in Fig. 5. Results for solid-state reactions with TCP and HA are provided in supplementary Figs. S19 and S20. With three exceptions, all reactions were found to be thermodynamically favourable at all temperatures. Unfavourable exceptions were the reactions TCP + CaO → TetCP, HA + CaO → TetCP, and below 600 K the reaction CPP + HA → TCP.

Based on the results of the thermodynamic calculations we derived a model for the cascade of reactions occurring during the thermal decomposition of CaP phases. In doing so, we limit ourselves to the consideration of the thermodynamic reaction energies and equilibrium vapour pressures and do not go further into kinetic aspects (activation energies, surface area, reaction rate constants, nucleation rate). Thus, our model does not allow any statement about the reaction rates and the temperature necessary to overcome the activation energy. However, we can deduce from it, which reactions are thermodynamically possible and in which direction they run. Furthermore, it can be assumed that the majority of commercial CaP products have undergone thermal treatment to improve their mechanical stability [13]. Since the high diffusion rates required for consolidation are only achieved at high temperatures [27], it can be assumed that the activation energy of all decomposition and solid state reactions is overcome. We therefore assume that all thermodynamically possible reactions take place during a common consolidation treatment when deriving our model for the thermal decomposition of CPP, TCP, HA and TetCP.

3.2. Decomposition model in open systems

A system is considered open if fresh air supply is sufficient to keep the vapour pressure of all decomposition reactions below saturation at all times. This can be maintained by forced ventilation of the furnace or by sintering in a hot air flow or over an open flame. Our model starts with the decomposition of CPP, which is the most phosphate-rich phase of our system. According to the reaction energies ΔG_r, decomposition to TCP, HA, TetCP, and CaO occur. After onset of phosphate evaporation (Fig. 6A), we thus predict the formation of all four phosphate depleted phases on the surface of the CPP substrate (Fig. 6B). The role of TetCP is somewhat unclear: It can form as a product of CPP decomposition, but it is unstable and decomposes to TCP + CaO (Fig. S19) and HA + CaO (Fig. S20) at ambient humidity. For the sake of simplicity, it is therefore omitted in the following reaction cascade and discussed later in this work. The decomposition products TCP, HA, and CaO that formed on the surface of the CPP substrate (Fig. 6B) undergo further reactions: TCP and HA continue to decompose by phosphate evaporation, and HA and CaO are unstable in direct contact with CPP and thus undergo solid-state reactions with the CPP substrate (Fig. 6C). These processes continue as long as phosphate ions diffuse from the substrate to the surface, and as long as unstable phase associations exist in the surface layer. The actual formation and lifetime of the individual phosphate-depleted phases in the layer depend on a complex overlap of several kinetic factors. If the rates of phase-forming decomposition and solid-state reactions exceed the rates of phase-consuming reactions, the phase will persist and form a layer of growing thickness. Otherwise, the phase's lifetime is limited and it will not be a substantial part of the layer composition. Our model predicts that a gradient of phases as depicted in Fig. 6D is possible based on thermodynamic calculations. Kinetic aspects, however, may allow only a subset of these phases to persist and grow in thickness.

Decomposition by phosphate evaporation of TCP, HA, and TetCP follow the same principles and are in fact a subset of the processes presented in Fig. 6. The products of decomposition and solid-state reactions form a sequence of increasingly phosphate-depleted phases on the substrate. More specifically, if the substrate phase is TCP, the phosphate-depleted surface layer contains HA and CaO. On a HA substrate, the surface layer contains CaO, which is the only thermodynamically stable phase formed by the decomposition of HA.

3.3. Decomposition model for closed systems

In a closed system, the vapour pressure of evaporated P species can build up and reach equilibrium with the solid phases, which changes the predicted cascade of decomposition and solid-state reactions relative to the open system. Fig. 7 shows the saturation pressures of PO_2 for all decomposition reactions at 1300 K, which is close to the temperature used for the experimental verification. While the absolute equilibrium pressures vary with temperature, the relative values at 1300 K are representative for the entire modelled temperature range (Figs. 4 and S10–S18). Reaction numbers (1) to (6) shown in Fig. 7 will be used to reference the reactions in the following discussion.

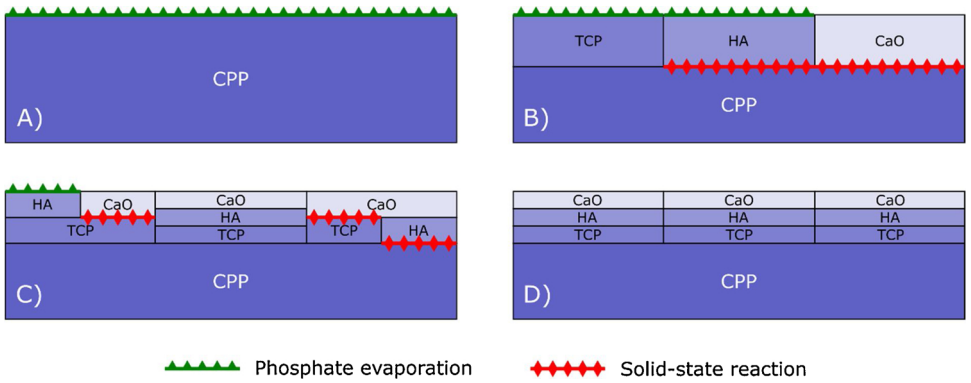

Fig. 6. Phosphate evaporation from a CPP substrate (A) calcined in an open system with a flushed atmosphere causes a cascade of decomposition and solid-state reactions (B, C), eventually leading to a gradient of increasingly Ca-rich phases from interior to the surface (D).

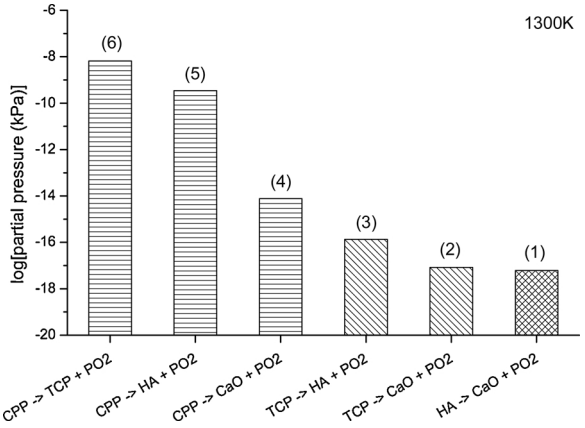

Fig. 7. Calculated PO_2 equilibrium vapour pressures at 1300 K for all decomposition reactions involving the phases CPP, TCP, HA, and CaO. Numbers in parentheses are used in the description of the model to address the individual reactions.

The sequence of reactions predicted by our model for CPP decomposition in a closed system is shown schematically in Fig. 8. In the early stages of decomposition, when none of the vapour pressures have reached equilibrium with the solid phases, our model for closed systems is identical to the open system. In other words, on a CPP substrate, all phosphate-depleted phases TCP, HA, CaO, and, depending on kinetics, TetCP, can form. We will again ignore the intermediate formation of TetCP for the reasons given previously. After the initial formation of TCP, HA, and CaO, secondary decomposition and solid-state reactions occur as discussed in the model for open systems (Fig. 8A). However, sustained phosphate evaporation in the closed system results in a gradual increase of the partial pressure of P species in the atmosphere. At some point, the partial pressure reaches equilibrium with reaction (1) and (2), but reactions (3)–(6) continue to release P species. The atmosphere thus becomes supersaturated towards reactions (1) and (2), which invert their direction and turn into condensation reactions. As a result, CaO reacts with P gas species to form HA and TCP (Fig. 8B). As the partial pressure further increases, reactions (3), (4), and (5) become supersaturated and revert their direction (Fig. 8C). Reaction (6) continues to release P species. Eventually, decomposition of the CPP substrate subsides when the partial pressure reaches equilibrium with reaction (6) (Fig. 8D). At this point, all intermediately formed HA, CaO, and potentially TetCP have been eliminated from the system by condensation with P gas species to form TCP and/or CPP. The system reaches a stable state when the surface layer on the CPP substrate consists of single-phase TCP, and the partial pressure of P gas species is in equilibrium with the reaction CPP = TCP + PO_2 (6).

The same principle of sequential surpassing of equilibrium partial pressures applies to substrates other than CPP. According to Fig. 7, a TCP substrate eventually reaches equilibrium with HA, as the system TCP = HA + PO_2 supersaturates the atmosphere for CaO and TetCP. Accordingly, HA substrates reach equilibrium with the system HA = CaO + PO_2. Similar to the open system, TetCP is thermodynamically unstable at the modelled conditions and is predicted to decompose to HA + CaO or TCP + CaO. The phases TCP and CaO, however, undergo a solid-state reaction to HA. TetCP substrates thus reach equilibrium when the substrate has completely transformed to HA + CaO and is in equilibrium with the partial pressure of the system HA = CaO + PO_2.

3.4. Experimental validation

3.4.1. Evaporation in open systems

Phase compositions of the samples exposed to 1373 K for 36 h in a ventilated furnace are shown in Table 2. Samples CaP1.0r showed a highly significant ($p < 0.01$) increase of β-TCP phase content from 1.1 ± 0.1 wt-% in the bulk to 25.2 ± 5.7 wt-% on the top surface. Accordingly, the Ca:P ratio increased from 1.0045 in the bulk to 1.108 on the top surface demonstrating that phosphate loss due to evaporation was relevant. At the same time, the bottom surface, which was in close contact with the second disks in the stack and thus shielded from the atmosphere, only formed 2.2 ± 1.2 wt-% β-TCP. The large variation of β-TCP content on the top surfaces was attributed to inhomogeneous ventilation in the furnace. As shown in Fig. 9, samples positioned in the line between the air inlet and outlet contained up to 35.4 wt-% β-TCP, whereas a sample on the opposite side merely reached 17.3 wt-% β-TCP. No phases other than β-TCP and the β-CPP substrate were detected. A depth profile of the Ca and P concentration determined by XPS confirmed an increase of the Ca:P ratio towards the surface (Fig. 10). Fitting the Ca:P values determined by XPS with an exponential function indicated that the molar ratio at the surface was close to 1.50, i.e. the

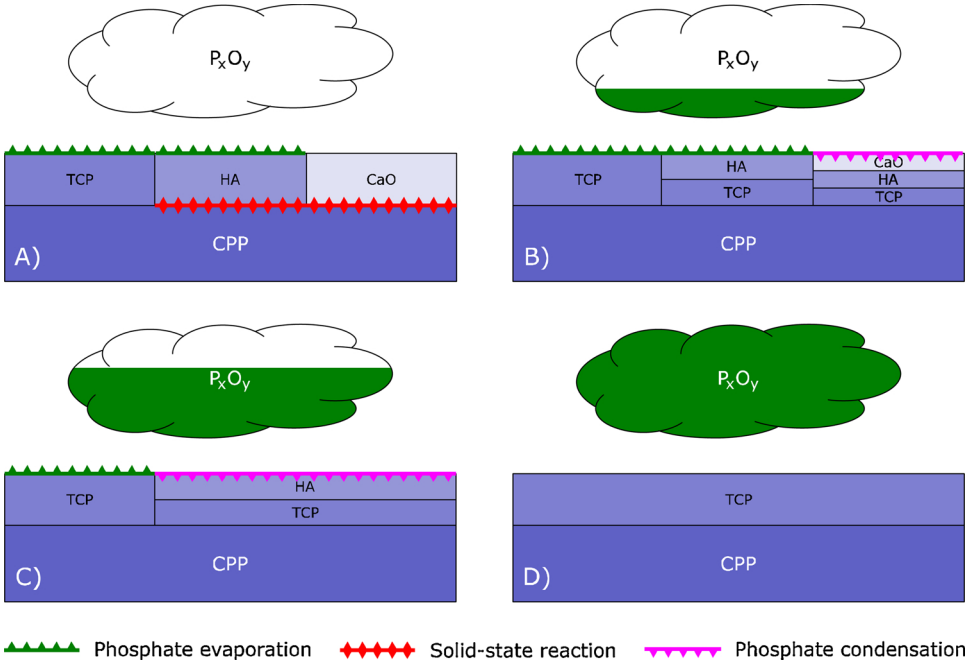

Fig. 8. Phosphate evaporation from a CPP substrate calcined in a closed system with a static atmosphere initially results in the formation of all phosphate-depleted solid phases (A). As the P_xO_y partial pressure in the atmosphere increases (represented by the increasing level of green in the cloud), it exceeds the equilibrium pressure for some decomposition reactions and thus causes phosphate condensation (B and C). The system reaches equilibrium when the atmosphere is in equilibrium with only the solid phases CPP and TCP (D).

Table 2
Phase composition in wt-% of disk samples after calcination at 1373 K in a flushed furnace. Errors represent one standard deviation in case of n > 1, and one estimated standard deviation reported by the Rietveld refinement software in case of n = 1. Relative densities after calcination and linear shrinkage factors were determined in triplicate (n = 3).

Sample	Bulk composition	Top Surface	Bottom Surface	Relative density (%)	Linear shrinkage (%)
CaP1.0r	β-CPP: 98.9 ± 0.1 β-TCP: 1.1 ± 0.1 Ca:P ratio: 1.0045 ± 0.0004 n: 1	β-CPP: 74.8 ± 5.7 β-TCP: 25.2 ± 5.7 Ca:P ratio: 1.108 ± 0.026 n: 10	β-CPP: 97.8 ± 1.2 β-TCP: 2.2 ± 1.2 Ca:P ratio: 1.009 ± 0.005 n: 10	86.9 ± 2.6	13.0 ± 0.2
CaP1.0p	β-CPP: 97.7 ± 0.4 β-TCP: 2.3 ± 0.4 Ca:P ratio: 1.010 ± 0.002 n: 3	β-CPP: 83.2 ± 1.6 β-TCP: 16.8 ± 1.6 Ca:P ratio: 1.071 ± 0.007 n: 3	β-CPP: n.a. β-TCP: n.a. Ca:P ratio: n.a. n: 3	69.8 ± 1.1	19.9 ± 0.2
CaP1.5	β-CPP: 1.7 ± 0.1 β-TCP: 98.3 ± 0.1 Ca:P ratio: 1.4900 ± 0.0007 n: 1	β-CPP: 0.4 ± 0.1 β-TCP: 99.6 ± 0.1 Ca:P ratio: 1.4977 ± 0.0006 n:6	β-CPP: 0.7 ± 0.3 β-TCP: 99.3 ± 0.3 Ca:P ratio: 1.4960 ± 0.0020 n: 6	66.8 ± 3.2	26.4 ± 0.5
CaP1.6	β-TCP: 33.5 ± 0.4 HA: 66.5 ± 0.4 Ca:P ratio: 1.6080 ± 0.0006 n: 1	β-TCP: 32.3 ± 0.6 HA: 67.7 ± 0.6 Ca:P ratio: 1.6101 ± 0.0010 n: 10	β-TCP: 33.8 ± 0.3 HA: 66.2 ± 0.3 Ca:P ratio: 1.6075 ± 0.0006 n: 10	55.8 ± 1.4	8.7 ± 0.2
CaP1.65	β-TCP: 18.0 ± 0.2 HA: 81.7 ± 0.2 CaO: 0.4 ± 0.1 Ca:P ratio: 1.6454 ± 0.0006 n: 1	β-TCP: 13.9 ± 2.7 HA: 85.6 ± 2.8 CaO: 0.5 ± 0.1 Ca:P ratio: 1.656 ± 0.003 n: 3	β-TCP: 18.2 ± 0.8 HA: 81.4 ± 0.7 CaO: 0.3 ± 0.4 Ca:P ratio: 1.644 ± 0.002 n: 3	39.9 ± 0.7	6.3 ± 0.02
CaP1.7	β-TCP: 2.6 ± 0.3 HA: 96.7 ± 0.3 CaO: 0.8 ± 0.1 Ca:P ratio: 1.685 ± 0.001 n: 1	β-TCP: 2.0 ± 1.2 HA: 96.6 ± 1.0 CaO: 1.4 ± 0.3 Ca:P ratio: 1.705 ± 0.011 n: 3	β-TCP: 2.8 ± 0.6 HA: 96.3 ± 0.6 CaO: 1.0 ± 0.1 Ca:P ratio: 1.690 ± 0.002 n: 3	42.9 ± 0.6	6.3 ± 0.05

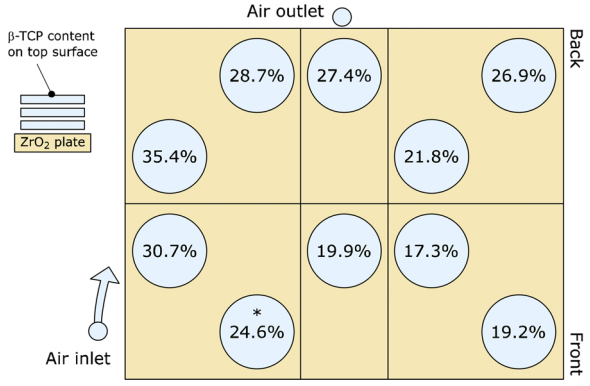

Fig. 9. The amount of β-TCP formed on the surface of CPP disks (CaP1.0r) strongly depended on the position of the samples relative to the air inlet and outlet. The sample marked with * was used for XPS analysis.

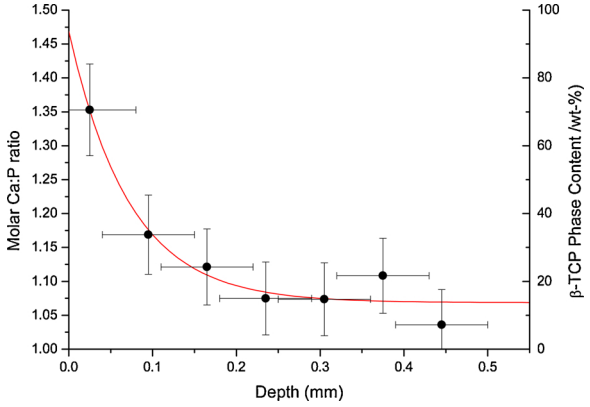

Fig. 10. A depth profile of the Ca:P ratio of material CaP1.0r calcined in an open system was determined by XPS. Horizontal error bars represent the beam spot size of 110 μm, vertical error bars represent estimated standard deviations of the XPS analysis (n = 1). An exponential decay curve fit (red line) resulted in R^2 = 0.9372.

value expected for pure β-TCP.

Pre-processing material CaP1.0p at 673 K converted the phase composition from DCPA to γ-CPP prior to the evaporation experiments and thus eliminated the release of H_2O in the furnace by the reaction 2 $CaHPO_4$ (DCPA) → $Ca_2P_2O_7$ (CPP) + H_2O from the verification experiments. Bottom surface compositions could not be determined from XRD data because excessive grain growth resulted in distorted XRD peak shapes and intensities. But a comparison with the bulk composition showed a highly significant ($p < 0.01$) increase of the β-TCP content from 2.3 ± 0.4 wt-% in the bulk to 16.8 ± 1.6 wt-% at the top surface (Table 2). Top surface compositions of individual samples again fluctuated strongly, indicating a high sensitivity to fresh air circulation and temperature inhomogeneities in the flushed furnace.

On CaP1.5 disks, the thermal treatment induced a statistically significant reduction of residual β-CPP on both surfaces as compared to the bulk ($p < 0.01$). A minor reduction ($p > 0.05$) of β-TCP from 0.7 ± 0.3 wt-% on the bottom to 0.4 ± 0.1 wt-% on the top surface was observed. No additional phases were detected.

Bi-phasic samples (CaP1.6 and CaP1.65) composed of a mixture of β-TCP and HA showed an increased HA content on the top surface, whereas the bottom surface did not show any significant change in phase composition relative to the bulk (Table 2). The HA increase of 1.2 wt-% on samples CaP1.6 was moderate but consistent and thus statistically significant ($p < 0.01$), whereas the increase of 3.9 wt-% on Samples CaP1.65 was insignificant ($p > 0.05$) due to strong position-related fluctuations. Traces of CaO were found in the bulk and on both surfaces of samples CaP1.65. Since this phase cannot coexist with β-TCP under the given processing conditions, it is presumed to be the residue of precursor material that could not react with β-TCP due to inhomogeneities in the precursor powder blend. Due to the limited sensitivity of the method, it was not possible to determine whether CaO had also been formed on the upper surface by evaporation in addition to the baseline contamination.

Samples CaP1.7 contained small amounts of β-TCP and CaO in the

Table 3
Phase composition in wt-% of disk samples after co-calcination with material CaP1.0r at 1373 K in a closed furnace. Errors represent one standard deviation in case of n > 1, and one estimated standard deviation reported by the Rietveld refinement software in case of n = 1.

Sample	Bulk composition	Top Surface	Bottom Surface
CaP1.5	β-CPP: 1.7 ± 0.1 β-TCP: 98-.3 ± 0.1 Ca:P ratio: 1.4900 ± 0.0007 n: 1	β-CPP: 2.3 ± 2.1 β-TCP: 97.9 ± 2.1 Ca:P ratio: 1.4859 ± 0.0124 n: 4	β-CPP: 1.3 ± 0.3 β-TCP: 98.7 ± 0.3 Ca:P ratio: 1.4923 ± 0.0018 n: 4
CaP1.6	β-TCP: 33.5 ± 0.4 HA: 66.5 ± 0.4 Ca:P ratio: 1.6080 ± 0.0006 n: 1	β-TCP: 50.2 ± 7.1 HA: 49.8 ± 7.1 Ca:P ratio: 1.5798 ± 0.0119 n: 4	β-TCP: 32.28 ± 0.04 HA: 67.72 ± 0.04 Ca:P ratio: 1.6100 ± 0.0001 n: 4
CaP1.65	β-TCP: 16.9 ± 0.2 HA: 83.0 ± 0.2 CaO: 0.14 ± 0.02 Ca:P ratio: 1.6407 ± 0.0006 n: 1	β-TCP: 39.9 ± 6.8 HA: 60.0 ± 6.8 CaO: 0.06 ± 0.03 Ca:P ratio: 1.599 ± 0.011 n: 3	β-TCP: 15.2 ± 4.0 HA: 84.5 ± 4.0 CaO: 0.28 ± 0.06 Ca:P ratio: 1.648 ± 0.009 n: 3
CaP1.7	β-TCP: 2.8 ± 0.2 HA: 96.5 ± 0.2 CaO: 0.70 ± 0.02 Ca:P ratio: 1.6827 ± 0.0003 n: 1	β-TCP: 5.4 ± 2.5 HA: 94.1 ± 2.3 CaO: 0.5 ± 0.3 Ca:P ratio: 1.673 ± 0.013 n: 3	β-TCP: 1.4 ± 0.4 HA: 97.6 ± 0.4 CaO: 1.01 ± 0.05 Ca:P ratio: 1.695 ± 0.002 n: 3
CaO	CaO:100.0 ± 0.0 n: 1	HA:14.8 ± 3.2 CaO:85.2 ± 3.2 Ca:P ratio: 19.6 ± 4.9 n: 4	HA:1.0 ± 0.2 CaO:99.0 ± 0.2 Ca:P ratio: 299.9 ± 46.4 n: 4

HA matrix in the bulk and on both surfaces. Since the same raw materials and preparation methods were used as for samples CaP1.65, we also assume that complete reaction of β-TCP with CaO was prevented by inhomogeneities. The top surface showed a reduction of β-TCP and an increase of CaO content (Table 2) relative to the bulk composition. The Ca:P ratio increased from 1.685 ± 0.001 in the bulk to 1.705 ± 0.011 on the upper surface.

3.4.2. Condensation in closed systems

The composition of disks calcined for 36 h at 1373 K in a closed furnace alongside with CaP1.0r powder is shown in Table 3. Samples CaP1.5 did not show any change in surface phase composition compared to the bulk. This was expected because the CaP1.5 phase composition (β-TCP with traces of β-CPP) was in equilibrium with the sacrificial CaP1.0r phase composition (β-CPP with traces of β-TCP). Co-calcination and closing the furnace thus effectively suppressed phosphate depletion of the surface as observed in the open system.

The bi-phasic disks CaP1.6 showed a significant ($p < 0.05$) reduction of the HA phase content at the top surface from 66.5 ± 0.4 wt-% in the bulk to 49.8 ± 7.1 wt-% at the surface. The large variations were again attributed to the position in the furnace. The bottom surface composition remained unchanged. A change of even greater extent was observed in samples CaP1.65, in which the HA content changed from 83.0 ± 0.2 wt-% in the bulk to 60.0 ± 6.8 wt-% at the top surface, while the β-TCP content increased by the same amount. The bottom surface remained unchanged relative to the bulk.

On the top surface of samples CaP1.7, phosphate condensation caused an insignificant increase of β-TCP and decrease of CaO ($p > 0.05$). Major phosphate condensation was observed on the top surface of pure CaO samples, resulting in the formation of 14.8 ± 3.2 wt-% HA ($p < 0.01$). Only traces of HA were formed on the bottom surface, and none was found in the bulk.

Two-way ANOVA was used to identify factors with a significant ($p \leq 0.05$) influence on the Ca:P ratio at the top surface relative to the bottom surface. In all samples, the position in the furnace (rear-left / center-center / front-right) was found to be insignificant ($p > 0.05$). The miniscule changes in Ca:P ratio of samples CaP1.5 and CaP1.7 in the open furnace, as well as CaP1.5 in the closed furnace, were also insignificant. All other observed changes in Ca:P ratio at the top surface, specifically on CaP1.0r, CaP1.0p, CaP1.6, and CaP1.65 in open atmosphere and CaP1.6, CaP1.65, CaP1.7, and CaO in closed atmosphere, were either significant ($p \leq 0.05$) or highly significant ($p \leq 0.01$). Individual p values are listed in Table S4.

3.4.3. Processing time and temperature

The effect of calcination time and temperature on phosphate evaporation was analysed on the top surface of CaP1.0r disks processed in a furnace flushed with fresh air, because these conditions provoked by far the strongest compositional change at the sample surface in our experimental setup. A variable processing time at a constant temperature of 1373 K (Fig. 11) and a variable processing temperature at a constant time of 36 h (Fig. 12) both demonstrated that the rate of β-TCP formation on the β-CPP substrate depends on the processing time and temperature. Prolonging the calcination time up to 72 h resulted in an asymptotic increase of β-TCP content converging at approximately 30 wt-%. Accordingly, increasing the processing temperature from 1073 K to 1373 K resulted in an exponential increase of β-TCP content. As observed before, the position of the samples relative to the airflow in the furnace had a major influence on the amount of evaporation at 1373 K.

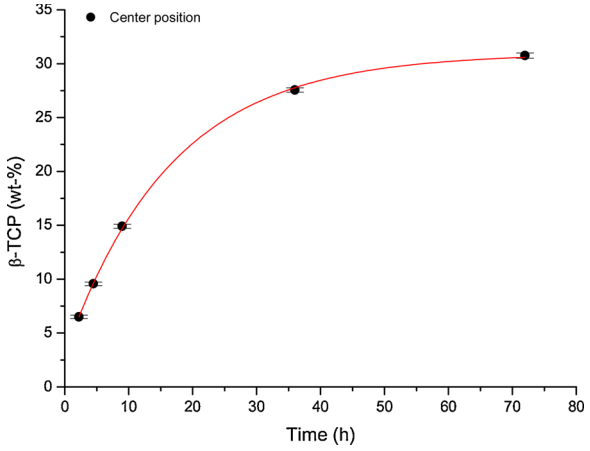

Fig. 11. Time-resolved formation of β-TCP on the top surface of β-CPP disks after calcination at 1373 K in a ventilated furnace. The samples (n = 1) were placed in the centre of the furnace. Error bars represent estimated standard deviations reported by the Rietveld refinement software. An asymptotic curve fit (red line) converged with $R^2 = 0.9995$.

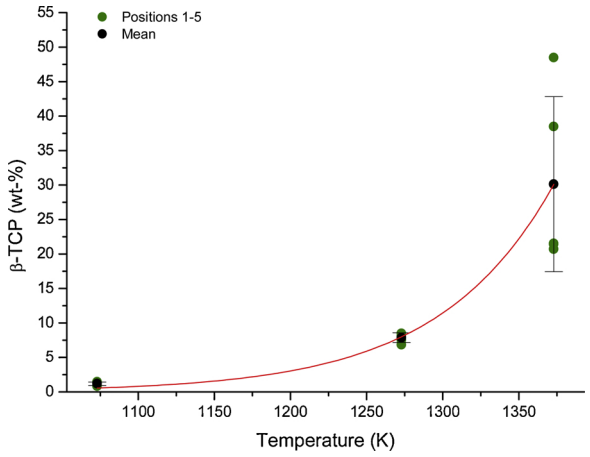

Fig. 12. The β-TCP phase content on the top surface of β-CPP disks calcined at different temperatures for 36 h in a ventilated furnace. Error bars represent one standard deviation (n = 5). Positions 1–4 were located in the corners of the furnace, position 5 in the centre. An exponential curve fit of the mean values (red line) converged with R^2 = 0.9982.

4. Discussion

4.1. Thermodynamic model

The aim of this study was to present a model for the evaporation of phosphate from the surface of CaP samples processed at high temperature based on thermodynamic data, and to discuss the effect of phosphate depletion on the surface phase composition. For this purpose, we calculated the Gibbs free energies of reaction of the decomposition reactions of CPP, TCP, HA, and TetCP (Table S1) on the basis of published Gibbs free energies of formation (Table S2). We found that a decomposition of all solid phases by release of different P gas phases can take place from room temperature onwards (Figs. 3 and S1–S9), provided that the activation energies of the reactions are surpassed and the atmosphere is undersaturated in P gas phases. For the released gas phases, we have calculated saturation vapour pressures in equilibrium with the solid reaction components (Figs. 4 and S10–S18). Based on published Gibbs free energies of formation of the solid phases, we calculated which of the phases formed by phosphate depletion react with each other or with the substrate (Table S3, Figs. 5, S19, S20). From the results of our calculations, we derived a model for the formation of a phosphate-depleted surface layer on CaP implants. Open (fresh air-flooded, Fig. 6) and closed furnaces (Fig. 8) had to be considered independently, since an increase of the P-vapour pressure in the closed system leads to a different growth characteristic and phase composition of the surface layer compared to a ventilated system (Fig. 7). To verify our models experimentally, we heat-treated samples of different raw materials (Table 1) using the setup shown in Fig. 1, and analysed the surface composition by XRD and XPS. Phosphate condensation from an oversaturated atmosphere was verified in a closed system (Fig. 2), and the effect of processing time and temperature on the layer formation was analysed.

We assumed a constant H_2O vapour pressure of 1.50 kPa in the atmosphere, which is the absolute amount of H_2O contained in an atmosphere of 50 % relative humidity at 298 K. Oxygen vapour pressure was set to 20.95 kPa, which represents the average oxygen content in the atmosphere. This atmospheric composition was assumed to represent an air-flushed furnace atmosphere. In a closed system, the O_2 and H_2O partial pressures may gradually change as the decomposition reactions proceed to release O_2 and release or consume H_2O (Table S1). The extent of these changes depends on the ratio of solid material to atmospheric volume in the furnace. Repeating the thermodynamic calculations using partial pressures of 10 and 90 kPa for O_2, and 0.15 and 3.0 kPa for H_2O (equivalent to 5–100% relative humidity at 298 K), revealed that the effect on Gibbs free energies of reactions ΔG_r and saturation vapour pressures were minor (not shown). Specifically, these changes to the atmosphere composition did not change the relative order of saturation vapour pressures, and none of the ΔG_r values changed the sign. Since these are the primary parameters our thermodynamic models are based on, the models are valid for atmospheres containing 10–90 kPa O_2, and 0.15–3.0 kPa H_2O. However, for atmospheres deviating significantly from these compositions, e.g. due to N_2 flushing, our thermodynamic models may not apply.

The formation and growth rate of the phosphate-depleted surface layer is based on decomposition reactions of the substrate and diffusion of the released molecules from the reaction front through the layer to the surface. The growth process of the layer is therefore very similar to the formation of an oxide layer on a metallic substrate, the growth of which is described by a model published by Deal and Grove [28,29]. This model establishes a relationship between the substrate oxidation rate, the oxygen diffusion flux, the processing time, and the layer thickness. If the growth rate of the layer is limited by the oxidation rate, there is a linear relationship between the layer thickness and the processing time. If the diffusion rate of oxygen through the surface layer is the limiting factor, the relationship between processing time and layer thickness is parabolic. A combination of linear and parabolic rate constant occurs when the growth rate is reaction limited at the beginning of the formation, but changes to diffusion-limited growth with increasing layer thickness. The Deal-Grove model not only applies to the diffusion of oxygen from the surrounding atmosphere through a surface oxide layer. Ions migrating in opposite direction from the substrate through the surface layer to the atmosphere follow the same principles [29,30]. According to Fick's first law of diffusion, the driving force for ion diffusion through the surface layer is a concentration gradient within the layer, specifically between the interfaces layer-to-substrate and layer-to-atmosphere [31]. By expelling the volatile P-species from the furnace in an open system, the concentration gradient of P gas species is maintained and the growth of the layer is thus limited by the reaction and diffusion rates. A closed system, on the other hand, reaches equilibrium when the increase of the P partial pressure in the atmosphere balances the gradient and thus the diffusion flux ceases. The application of these principles to porous materials in open systems is complicated by the fact that the gas concentrations within the pores may be higher than in the open furnace atmosphere due to limited gas transport through the pore system towards the sample surface. If the kinetics of the evaporation reaction is faster than the transport rate of gas through the pore system by diffusion and convection, the growth rate of the surface layer is limited by the gas transport rate. Taking this additional limitation into account, the model of Deal-Grove and Fick's Law confirm the prediction of our model for P evaporation from CaP phases regarding the different layer growth in open and closed systems.

4.2. Experimental validation

The materials used for experimental verification were of bi-phasic bulk composition, on which we could observe relative phase changes at the surface as an effect of phosphate evaporation or condensation without having to overcome a potential kinetic barrier of nucleating a new phase first. This allowed us to focus on thermodynamic aspects and minimize interference by nucleation, a kinetic effect that was outside the scope of this study.

A gradient of phosphate-depleted phases as expected for the open system was not observed experimentally. According to the XRD results, the surface layer of CPP samples (materials CaP1.0r and CaP1.0p) processed in the open furnace was composed of β-TCP only (Table 2). A depth profile of the Ca and P concentrations on CaP1.0r measured by XPS near the sample surface confirmed that the Ca:P ratio increased towards the surface, but did not exceed 1.50 (Fig. 10). Hence, neither XRD nor XPS results indicated the presence of a phase more depleted in

phosphate than β-TCP in the surface layer of β-CPP.

A strong dependence of the phosphate evaporation on the position of the samples relative to the fresh airflow was observed in the experiment in the open system. On CaP1.0r samples positioned close to the airflow, significantly more β-TCP was formed than on samples placed in the opposite corner of the furnace (Fig. 9). This indicates that despite the supply of fresh air, layer growth was limited by saturation of the atmosphere and our experimental setup did not represent an open system as presumed for our evaporation model. Instead, it was a semi-open system in which an increase in P-partial pressure resulted in a layer composition similar to the one predicted for closed systems. However, by evacuating the saturated atmosphere, the surface layer could grow to a greater thickness than in a static atmosphere, as demonstrated by the observed position dependence in our experiment. An open furnace in the sense of our model may be difficult to realize with conventional sintering furnaces, because an excessive flow of fresh air would affect the homogeneity and stability of the temperature.

Pre-processing raw material CaP1.0p at 673 K prior to the evaporation experiments to pre-empt the release of H_2O and maintain a constant absolute humidity in the furnace atmosphere had no major effect on the observed phase composition of the top surface. Both series of samples CaP1.0r (raw) and CaP1.0p (pre-treated) formed substantial amounts of β-TCP as a result of phosphate evaporation. These results confirmed the prediction of our model that phosphate evaporation is largely unaffected by the H_2O partial pressure in the furnace atmosphere and occurs in a wide range of absolute humidity.

Our verification experiments in an open furnace atmosphere covered a wide range of initial Ca:P ratios from 1.0 to 1.7, including most phases relevant for biomedical application. All samples showed a shift of the upper surface Ca:P ratio towards more Ca-rich values when processed at 1373 K, albeit to widely varying degrees (Table 2). The predicted formation of CaO as a result of thermal treatment of HA is often described in the literature [32,33], but it is not usually associated with evaporation of phosphate at the surface. Instead, CaO contamination is interpreted as a Ca excess in the bulk composition [34]. Based on our findings, we expect at least for a part of the reported CaO formations that the cause is phosphate evaporation. The extent of the chemical change depends strongly on material properties (initial phase composition, specific surface area, chemical contaminations) and process parameters (furnace permeability, active fresh-air supply, volume of the furnace chamber). Since the changes are concentrated at the surface, care is required especially when the thermal treatment of the implant is the last step and no homogenization or mechanical removal of the surface takes place afterwards. In this case, even thin chemically modified surface layers can strongly influence the biological behaviour of the implant.

The second round of experiments was conducted to assess the effect of a closed atmosphere supersaturated with P gas species towards the solid phases. Supersaturation towards TCP, HA, and CaO substrates was achieved by placing sacrificial CPP material in the furnace alongside the samples. According to the calculated equilibrium partial pressures of volatile P-species, the decomposition of CPP to TCP supersaturated the atmosphere towards any other decomposition reaction involving the phases CPP, TCP, HA, TetCP, and CaO (Fig. 7). As predicted by the model, phosphate enrichment was observed on the top surfaces of the TCP, HA, and CaO samples (Table 3), thus proving that condensation of P species from a supersaturated atmosphere changes the surface towards a more phosphate rich composition.

Over the past 20 years, the osteoinductive potential of CaP implants has been a much discussed subject [35–37]. Despite the vast majority of CaP implants being only osteoconductive, several studies observed ectopic bone formation in CaP granules and scaffolds and thus concluded that inorganic CaP implants can be osteoinductive, contrary to the general consensus [38,39]. Recently, Bohner and Miron [40] hypothesized that an optimum surface composition, surface topography, and scaffold architecture can trigger the differentiation of mesenchymal stem cells into the osteogenic lineage. According to their theory, the differentiation is initiated by a gradient of Ca concentration in the vicinity of the implant. A drop in Ca concentration near the implant surface can be the result of precipitation of biomimetic apatite on the surface, a process referred to as bioactivity according to Kokubo's definition [41]. Maazouz et al. [42] demonstrated that the surface composition, specifically soluble surface layers of CaO, $Ca(OH)_2$, and $CaCO_3$, strongly affected the kinetics of apatite precipitation on the implant surface by increasing the local Ca concentration and supersaturating the extracellular fluid. These authors thus proposed a direct relation between surface composition, bioactivity, and osteoinductive potential of inorganic CaP materials, as hypothesized by Bohner and Miron and as observed in various studies before [21,43–45]. In this respect, the formation of large amounts of HA on the CaO sample observed in the supersaturated atmosphere was of particular interest. CaO reacts with ambient humidity to $Ca(OH)_2$, and further to $CaCO_3$ by carbonization with atmospheric CO_2 [46]. These phases dissolve quickly after implantation and result in a burst release of Ca and an increase of the pH value [47–49]. A moderate increase of pH was described to have a positive regulatory effect on osteoblast activity in osteoporotic patients [50–52], but a rapid decline in activity was observed at pH 8.8 and higher [53]. Placing sacrificial CPP material in the furnace alongside with samples containing CaO at the surface offered the possibility of converting CaO into HA by phosphate condensation and thus regulating the amount of soluble CaO, $Ca(OH)_2$, and $CaCO_3$ at the implant surface.

4.3. Solid-state reactions

The Gibbs free energies of reaction ΔG_r for solid-state reactions we present in Figs. 5, S19, and S20 indicate that HA is stable up to 1700 K in air atmosphere, and that TetCP can be formed by the reaction CPP + CaO, but decomposes to TCP and/or HA. These findings seem to contradict previous reports of HA decomposition and successful formation of TetCP in air atmosphere, which is why we discuss them below.

The decomposition of HA into CaO and α-TCP by high energy input, for example by thermal treatment [54,55], plasma spraying [56,57], or high-energy irradiation under vacuum [58] is occasionally described in the literature. According to our calculations, a direct decomposition of HA into TCP + CaO is thermodynamically not possible at temperatures up to 1700 K, 100 kPa atmospheric pressure, and 1.50 kPa H_2O vapour pressure (Fig. S19). However, the studies referenced above describe samples that either had not reached a thermodynamic equilibrium, or were processed under conditions different from ambient pressure. Pazarhoglu and Salman [54] found β- and α-TCP after calcination at 1573 K, but only 0.1 wt-% CaO, which is at the detection limit of conventional XRD instruments. Pham et al. [55] describe CaO and α-TCP phases coexisting with HA as residual precursor phases that were unable to react due to inhomogeneities in the sample. The sample had thus not reached thermodynamic equilibrium. The composition of plasma-sprayed coatings is dominated by the kinetics of crystallization from a melt. The rapid cooling rate again prevents the samples from reaching a thermodynamic equilibrium. The last group of observations of HA decomposition were made under high-vacuum in an electron microscope while irradiating the sample with an electron beam. The atmospheric conditions are vastly different from the atmospheric conditions our thermodynamic models were calculated for, hence the models may not apply for the different experimental conditions. One pathway for HA decomposition in air atmosphere was proposed by Cihlář et al. [59], who showed that decomposition to CaO and TCP can occur at high temperature if HA is first converted to hydroxyoxyapatite (HOA) or oxyapatite (OA, $Ca_{10}(PO_4)_6O$). The same decomposition process was described by Zhou et al. [60]. The dehydroxylation temperature of HA is known to strongly correlate with the H_2O vapour pressure in the atmosphere [61]. We did not calculate Gibbs free energies of reaction ΔG_r for the dehydroxylation of HA due to its complex divariant and

progressive characteristic.

Cieśla and Rudnicki investigated the formation of TetCP by solid-state reaction in a series of publications. According to their first study [62], the reaction CPP + CaO → TetCP in air produced TetCP alongside with HA and TCP at 1573 K, and phase-pure TetCP at 1673 K. These temperatures were reduced by approximately 100 K when the experiments were repeated in a purified N_2 stream. According to our calculations of ΔG_r, this was the only solid-state reaction capable of producing TetCP in air (Fig. 5). Reactions of TCP + CaO → TetCP (Fig. S19) and HA + CaO → TetCP + H_2O (Fig. S20) are thermodynamically unfavourable. The authors reported in a follow-up study [63] that TCP + CaO in air reacted to HA, followed by a weight loss above 1500 K. It was not determined whether the weight loss was related to TetCP formation or dehydroxylation of HA. TetCP was obtained from both reactions in purified N_2 atmosphere. The experimental results of TetCP formation in air atmosphere presented by Cieśla and Rudnicki are thus in good agreement with our thermodynamic calculations.

With the new insight in phosphate evaporation and condensation we present in this study, and specifically their sensitivity to environmental factors, we now understand why samples of identical bulk composition, scaffold architecture, and surface topography can provoke substantially different in-vivo responses at the defect site [18–23]. For precise control of the surface composition, technical aspects such as the permeability of furnace chambers, active fresh air supply, the ratio of sample volume to total furnace volume, and mechanical shaping applied pre- or post-sintering must be taken into account. At the same time, controlled ventilation or supersaturation of the furnace atmosphere allow us to steer the surface composition in the desired direction anywhere from phosphate-depletion to phosphate-enrichment to optimize the biological performance of the implants.

5. Conclusion

A thorough assessment of the thermodynamic properties of high-temperature CaP phases allowed us to establish a model for chemical surface modification induced by phosphate evaporation and condensation during high-temperature treatment. The model was confirmed by a series of experiments, which demonstrated that phosphate depletion at the surface of a variety of CaP phases occurred at 1373 K. Furthermore, our new findings suggest that the thickness and composition of the phosphate-depleted surface layer depends on a number of process parameters such as the volume and loading of the furnace, or its ventilation and permeability. Our thermodynamic model enables us to understand the nature of the chemical surface changes and to use them to our advantage. For example, it was demonstrated that phosphate depletion can be suppressed and even inverted by co-sintering the implants alongside with sacrificial CaP material used to supersaturate the atmosphere. The surface composition of CaP implants, specifically the solubility of the surface phases and their dissolution kinetics, their influence on the pH value, and their effect on bioactivity, plays a critical role in the biological performance of the implant. Our model for temperature-induced chemical surface modification facilitates the development of CaP implants with more consistent and optimized biological performance.

Declaration of Competing Interest

The authors declare that they have no known competing financial interests or personal relationships that could have appeared to influence the work reported in this paper.

Acknowledgement

The authors would like to thank Janine Glatthard for her tremendous support with the verification experiments.

Appendix A. Supplementary data

Supplementary material related to this article can be found, in the online version, at doi:https://doi.org/10.1016/j.jeurceramsoc.2020.07.028.

References

[1] D.G. Castner, B.D. Ratner, Biomedical surface science: foundations to frontiers, Surf. Sci. 500 (1–3) (2002) 28–60.
[2] L.L. Hench, E.C. Ethridge, Biomaterials - the interfacial problem, Adv. Biomed. Eng. 5 (1975) 35–150.
[3] M. Geetha, et al., Ti based biomaterials, the ultimate choice for orthopaedic implants - a review, Prog. Mater. Sci. 54 (3) (2009) 397–425.
[4] Y. Ikada, Surface modification of polymers for medical applications, Biomaterials 15 (10) (1994) 725–736.
[5] H. Zreiqat, P. Evans, C.R. Howlett, Effect of surface chemical modification of bioceramic on phenotype of human bone-derived cells, J. Biomed. Mater. Res. 44 (4) (1999) 389–396.
[6] V.P. Galván-Chacón, P. Habibovic, Deconvoluting the bioactivity of calcium phosphate-based bone graft substitutes: strategies to understand the role of individual material properties, Adv. Healthc. Mater. 6 (13) (2017).
[7] C. Rey, et al., Surface properties of biomimetic nanocrystalline apatites; applications in biomaterials, Prog. Cryst. Growth Charact. Mater. 60 (3-4) (2014) 63–73.
[8] D. Eichert, et al., Formation and evolution of hydrated surface layers of apatites, Key Eng. Mater. 284–286 (2005) 3–6.
[9] J.M. Bouler, R.Z. LeGeros, G. Daculsi, Biphasic calcium phosphates: influence of three synthesis parameters on the HA/beta-TCP ratio, J. Biomed. Mater. Res. 51 (4) (2000) 680–684.
[10] M. Bohner, Resorbable biomaterials as bone graft substitutes, Mater. Today 13 (1-2) (2010) 24–30.
[11] M. Draenert, A. Draenert, K. Draenert, Osseointegration of hydroxyapatite and remodeling-resorption of tricalciumphosphate ceramics, Microsc. Res. Tech. 76 (4) (2013) 370–380.
[12] S.A. Clarke, et al., Surrogate outcome measures of in vitro osteoclast resorption of β tricalcium phosphate, Adv. Healthc. Mater. 6 (1) (2017).
[13] E. Champion, Sintering of calcium phosphate bioceramics, Acta Biomater. 9 (4) (2013) 5855–5875.
[14] ISO, ISO 13779-3:2018 - Implants for Surgery - Hydroxyapatite; Part 3: Chemical Analysis and Characterization of Crystallinity and Phase Purity, (2018) Geneva, Switzerland.
[15] J.H. Welch, W. Gutt, High-temperature studies of the system calcium oxide-phosphorus pentoxide, J. Chem. Soc. 874 (1961) 4442–4444.
[16] T. Nagai, M. Miyake, M. Maeda, Thermodynamic measurement of calcium phosphates by double Knudsen cell mass spectrometry, Metal. Mater. Trans. B: Process Metal. Mater. Process. Sci. 40 (4) (2009) 544–549.
[17] T. Nagai, Y. Tanaka, M. Maeda, Thermodynamic measurement of di-calcium phosphate, Metal. Mater. Trans. B: Process Metal. Mater. Process. Sci. 42 (4) (2011) 685–691.
[18] C. Ribeiro, et al., Formation of calcium phosphate layer on ceramics with different reactivities, Mater. Sci. Eng. C 24 (5) (2004) 631–636.
[19] R. Xin, et al., A comparative study of calcium phosphate formation on bioceramics in vitro and in vivo, Biomaterials 26 (33) (2005) 6477–6486.
[20] A. Barba, et al., Osteoinduction by foamed and 3D-printed calcium phosphate scaffolds: effect of nanostructure and pore architecture, ACS Appl. Mater. Interfaces 9 (48) (2017) 41722–41736.
[21] M. Tsukanaka, et al., Osteoinductive potential of highly purified porous β-TCP in mice, J. Mater. Sci. Mater. Med. 26 (3) (2015).
[22] R. Duan, et al., Variation of the bone forming ability with the physicochemical properties of calcium phosphate bone substitutes, Biomater. Sci. 6 (1) (2018) 136–145.
[23] N.L. Davison, et al., Osteoclast resorption of beta-tricalcium phosphate controlled by surface architecture, Biomaterials 35 (26) (2014) 7441–7451.
[24] M. Bohner, et al., Effect of thermal treatments on the reactivity of nanosized tricalcium phosphate powders, J. Mater. Chem. 18 (37) (2008) 4460–4467.
[25] R.J. Egli, et al., Thermal treatments of calcium phosphate biomaterials to tune the physico-chemical properties and modify the in vitro osteoclast response, Adv. Eng. Mater. 13 (3) (2011) B102–B107.
[26] N. Doebelin, R. Kleeberg, Profex: a graphical user interface for the Rietveld refinement program BGMN, J. Appl. Crystallogr. 48 (5) (2015) 1573–1580.
[27] S. Raynaud, E. Champion, D. Bernache-Assollant, Calcium phosphate apatites with variable Ca/P atomic ratio II. Calcination and sintering, Biomaterials 23 (4) (2002) 1073–1080.
[28] B.E. Deal, A.S. Grove, General relationship for the thermal oxidation fo silicon, J. Appl. Phys. 36 (12) (1965) 3770–3778.
[29] Y. Song, et al., Modified Deal Grove model for the thermal oxidation of silicon carbide, J. Appl. Phys. 95 (9) (2004) 4953–4957.
[30] S. Dimitrijev, H. Harrison, D. Sweatman, Extension of the deal-grove oxidation model to include the effects of nitrogen, IEEE Trans. Electron Devices 43 (2) (1996) 267–272.
[31] H.J.V. Tyrrell, The origin and present status of Fick's diffusion law, J. Chem. Educ. 41 (7) (1964) 397.
[32] A. Sobczak-Kupiec, Z. Wzorek, The influence of calcination parameters on free

calcium oxide content in natural hydroxyapatite, Ceram. Int. 38 (1) (2012) 641–647.
[33] J. Horng Yih, H. Min Hsiung, Fabrication and mechanical properties of hydroxyapatite-alumina composites, Mater. Sci. Eng. C 2 (1–2) (1994) 77–81.
[34] S. Raynaud, et al., Calcium phosphate apatites with variable Ca/P atomic ratio I. Synthesis, characterisation and thermal stability of powders, Biomaterials 23 (4) (2002) 1065–1072.
[35] Z. Tang, et al., The material and biological characteristics of osteoinductive calcium phosphate ceramics, Regen. Biomater. 5 (1) (2018) 43–59.
[36] P. Habibovic, K. de Groot, Osteoinductive biomaterials–properties and relevance in bone repair, J. Tissue Eng. Regen. Med. 1 (1) (2007) 25–32.
[37] R.Z. LeGeros, Calcium phosphate-based osteoinductive materials, Chem. Rev. 108 (11) (2008) 4742–4753.
[38] H. Yuan, et al., Osteoinduction by calcium phosphate biomaterials, J. Mater. Sci. Mater. Med. 9 (12) (1998) 723–726.
[39] T. Miramond, et al., Osteoinduction of biphasic calcium phosphate scaffolds in a nude mouse model, J. Biomater. Appl. 29 (4) (2014) 595–604.
[40] M. Bohner, R.J. Miron, A proposed mechanism for material-induced heterotopic ossification, Mater. Today 22 (2019) 132–141.
[41] T. Kokubo, Bioactive glass ceramics: properties and applications, Biomaterials 12 (2) (1991) 155–163.
[42] Y. Maazouz, et al., In vitro measurement of the chemical changes occurring within β-tricalcium phosphate bone graft substitutes, Acta Biomater. 102 (2020) 440–457.
[43] R.J. Miron, et al., Osteoinductive potential of a novel biphasic calcium phosphate bone graft in comparison with autographs, xenografts, and DFDBA, Clin. Oral Implants Res. 27 (6) (2016) 668–675.
[44] N.L. Davison, et al., Influence of surface microstructure and chemistry on osteoinduction and osteoclastogenesis by biphasic calcium phosphate discs, Eur. Cell. Mater. 29 (2015) 314–329.
[45] L. Wang, et al., Effect of particle size on osteoinductive potential of microstructured biphasic calcium phosphate ceramic, J. Biomed. Mater. Res. - Part A 103 (6) (2015) 1919–1929.
[46] M. Galván-Ruiz, et al., Characterization of calcium carbonate, calcium oxide, and calcium hydroxide as starting point to the improvement of lime for their use in construction, J. Mater. Civ. Eng. 21 (11) (2009) 694–698.
[47] S.L. Goss, et al., Determination of calcium salt solubility with changes in pH and P_{CO2} simulating varying gastrointestinal environments, J. Pharm. Pharmacol. 59 (11) (2007) 1485–1492.
[48] G. Vereecke, J. Lemaitre, Calculation of the solubility diagrams in the system Ca$(OH)_2$-H_3PO_4-KOH-HNO_3-CO_2-H_2O, J. Cryst. Growth 104 (1990) 820–832.
[49] H.A. Roth-Bassell, F.M. Clydesdale, In vitro solubility characteristics of six calcium salts, J. Food Prot. 55 (12) (1992) 1003–1005.
[50] H.C. Blair, et al., Support of bone mineral deposition by regulation of pH, Am. J. Physiol.-Cell Physiol. 315 (4) (2018) C587–C597.
[51] Y. Shen, et al., Interfacial pH: a critical factor for osteoporotic bone regeneration, Langmuir 27 (6) (2011) 2701–2708.
[52] W. Liu, et al., Alkaline biodegradable implants for osteoporotic bone defects—Importance of microenvironment pH, Osteoporos. Int. 27 (1) (2016) 93–104.
[53] A.-M. Galow, et al., Increased osteoblast viability at alkaline pH in vitro provides a new perspective on bone regeneration, Biochem. Biophys. Rep. 10 (2017) 17–25.
[54] S. Pazarlıoglu, S. Salman, Sintering effect on the microstructural, mechanical, and in vitro bioactivity properties of a commercially synthetic hydroxyapatite, J. Aust. Ceram. Soc. 53 (2) (2017) 391–401.
[55] D. Pham Minh, et al., Thermal behavior of apatitic calcium phosphates synthesized from calcium carbonate and orthophosphoric acid or potassium dihydrogen orthophosphate, J. Therm. Anal. Calorim. 112 (3) (2013) 1145–1155.
[56] M.T. Carayon, J.L. Lacout, Study of the Ca/P atomic ratio of the amorphous phase in plasma-sprayed hydroxyapatite coatings, J. Solid State Chem. 172 (2) (2003) 339–350.
[57] K.A. Khor, P. Cheang, Plasma sprayed hydroxyapatite(HA) coatings produced with flame spheroidised powders, J. Mater. Process. Technol. 63 (1-3) (1997) 271–276.
[58] A.V. Kostyuchenko, G.S. Kochlar, V.M. Ievlev, Electron irradiation effect in surface modification of hydroxyapatite ceramics, Inorg. Mater. 55 (12) (2019) 1285–1289.
[59] J. Cihlář, A. Buchal, M. Trunec, Kinetics of thermal decomposition of hydroxyapatite bioceramics, J. Mater. Sci. 34 (24) (1999) 6121–6131.
[60] J.M. Zhou, et al., High-temperature characteristics of synthetic hydroxyapatite, J. Mater. Sci.-Mater. Med. 4 (1) (1993) 83–85.
[61] K.A. Gross, L. Pluduma, Putting oxyhydroxyapatite into perspective: a pathway to oxyapatite and its applications, Calcium Phosphate: Structure, Synthesis, Properties, and Applications, Nova Science Publishers, Inc., 2012, pp. 95–120.
[62] K. Ciesla, R. Rudnicki, Synthesis and transformation of tetracalcium phosphate in solid-state.1. Synthesis of roentgenographically pure tetracalcium phosphate from calcium dibasic phosphate and calcite, Pol. J. Chem. 61 (7–12) (1987) 719–727.
[63] K. Ciesla, R. Rudnicki, Synthesis and transformations of tetracalcium phosphate in solid-state. 2. Studies on synthesis of tetracalcium phosphate by the thermal-analysis method, Pol. J. Chem. 62 (1-3) (1988) 31–39.